Available online at www.sciencedirect.com
SCIENCE DIRECT®
International Journal of Heat and Mass Transfer 49 (2006) 3130–3141
International Journal of HEAT and MASS TRANSFER
www.elsevier.com/locate/ijhmt

Design criteria for ribbed channels: Experimental investigation and theoretical analysis

Bruno Facchini, Luca Innocenti, Marco Surace *

Dipartimento di Energetica "Sergio Stecco" Universitá degli Studi di Firenze Via Santa Marta, 3 50139 Firenze, Italy

Received 21 February 2005
Available online 17 April 2006

Abstract

The present study investigates heat transfer and pressure drop in flows through ribbed channel for application to turbine blade cooling. The experiments are conducted for different cross-sections, for Reynolds number from 20 to 60×10^3. Local heat transfer coefficients are obtained using a transient thermochromic liquid crystal (TLC) technique. Detailed knowledge of the local heat transfer coefficient is essential to analyze thermal stresses in turbine components, while the combined effect of heat transfer and pressure drop should be taken into account for a proper cooling system design. As a compromise has always to be found, a new design criteria to choose the most appropriate solution for typical turbomachinery parameters is inferred and shown. Entrance effects for ribbed channels are also studied, as the common hypothesis of fully developed flow is rarely satisfied in real engine geometries; relevant results are revealed.

1. Introduction

The aim to reach higher and higher efficiency levels for turbogas engines, so as to reduce energy resources consumption and global emissions, pushed towards a gradual increase of maximum cycle temperature. At the same time, a constant search for new materials and casting techniques allowing to increase metal temperature, as well as the development and improvement of always more effective though complex cooling configurations is being carried out to ensure the required system reliability. Among various cooling techniques, turbulence promoters (ribs) are probably one of the most diffused, thanks to their ability to combine high heat transfer coefficients (mainly due to the increase of near wall flow turbulence level) to limited pressure losses.

Ribs as turbulence promoters have been employed in blade internal cooling channel since early 1970s, when several researchers, e.g., Han et al. [1] and Webb et al. [2], published their first results on such cooling systems, pointing out at the main features and advantages: briefly, fairly high performances with low structural complexity. Since then, several experimental (and recently also numerical) analyses have been performed on stationary and rotating channels ([3–8], allowing to better understand fluid dynamical phenomena related to such systems, while revealing still significant improvement margins for different rib configurations, in terms of shape and arrangement (Taslim [9], Hwang [10]). Practical importance of such technique is evident considering its wide utilization inside cooling channels of blade and vane, as soon as heat transfer enhancement is required (Fig. 1).

It is well known that heat transfer performances of turbulators improve with increasing Reynolds number and aspect ratio, as well as pressure losses worsen, then requiring higher pumping power to provide the required coolant flow. The selection criterion normally employed to compare different configurations was developed by Webb et al. [11] for heat exchanger ducts, thus expressed in terms of quantities not always significant in blade cooling analysis. For such reasons, existing criterion was properly modified, suppressing some approximations not allowed and using as main parameters cooling efficiency and

* Corresponding author. Tel.: +39 055 4796 575; fax: +39 055 4796 342.
E-mail address: suro@brun.de.unifi.it (M. Surace).

0017-9310/$ - see front matter © 2006 Elsevier Ltd. All rights reserved.
doi:10.1016/j.ijheatmasstransfer.2006.02.026

Nomenclature

A	heat transfer area (m^2)
AR	channel aspect ratio
c	flow velocity (m/s)
c_p	constant pressure specific heat (J/kg K)
D_h	hydraulic diameter (m)
Δp	static pressure difference (Pa)
e	rib height (m)
f	friction factor
h	local heat transfer coefficient (W/m^2 K)
$\overline{h}$	average heat transfer coefficient (W/m^2 K)
L	investigated zone length (m)
M	mass velocity (ρc) (kg/m^2 s)
Nu	Nusselt number
p	pressure (Pa)
P	ribs pitch (m)
Q	heat transfer (W)
R	air constant (J/kg K)
Re	Reynolds number
S	Passage area (m^2)
St	Stanton number
TLC	thermochromic liquid crystals
x	distance from channel inlet (m)
W	pumping power (W)

Greek symbols

α	ribs angle (deg)
ϵ	cooling efficiency
ϕ	cooling effectiveness
μ	dynamic viscosity (kg/m s)
ρ	Density (kg/m^3)

Subscripts

a	ambient conditions
b	blade
c	coolant conditions
d	discharge conditions
g	hot gases
o	outlet conditions
s	fully developed flow
sm	smooth channel
w	wall

effectiveness, commonly adopted to report cooling system performances.

Another interesting aspect of ribbed channels, often neglected, is related to the evaluation of entrance effect on heat transfer performances: commonly, most design process stages are carried out using data for fully developed flow, as they are thought to be conservative with respect to the foreseen increase due to the entrance effect. This aspect has been carefully investigated with specific experiments, whose results are later shown.

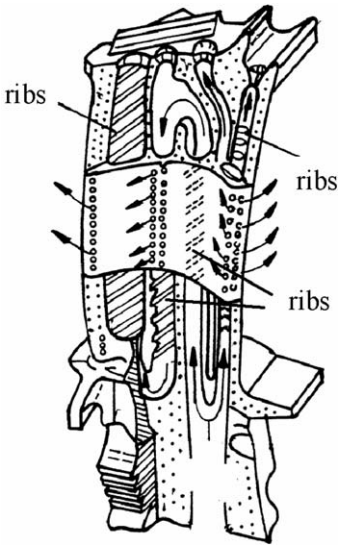

Fig. 1. Blade internal multi-pass cooling system.

2. Experiments

2.1. Test facility

The test facility (Fig. 2) is an open-loop suction type wind tunnel; this test rig allows heat transfer and pressure loss measurements on several kinds of test models. Air at atmospheric pressure and ambient temperature passes through a 9 kW electronically controlled electric heater to reach and keep a constant temperature, then the flow rate is measured by an orifice. A three way valve, with pneumatic actuator, can assure the sample at room temperature, as required when using TLC transient technique, while the other components of the test rig are warming up (during steady state tests, the valve is fixed). Two rotary vane vacuum pumps, powered by two 7.5 kW electric motors, blow air outside and provide a maximum mass flow rate of 0.16 kg/s. The flow rate is set up by guiding the motor

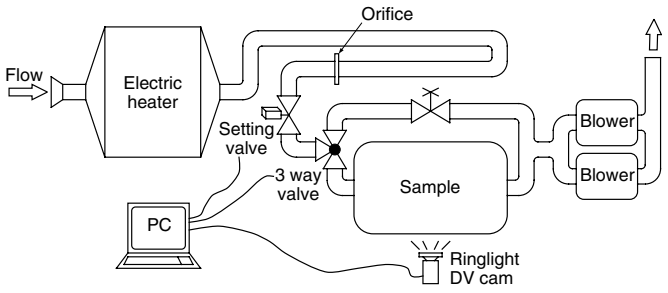

Fig. 2. Experimental setup.

speed between 300 and 1300 rpm and throttling a remote controlled motorized valve; the air temperature is controlled by means of a four wire RTD (Pt100). Three Scanivalve® DSA 3217 pressure scanners with temperature compensated piezoresistive relative pressure sensors allow to measure the total or static pressure in 48 different locations, with an accuracy of 6.9 Pa. A PC-linked data acquisition switch unit (HP/Agilent® 34970A) drives—in transient tests—the three way valve and synchronizes the video recording with the test start; moreover, it also measures the time dependent mainstream temperature by means of an external cold junction especially conceived for T type thermocouples. A digital 3CCD camcorder (Canon® XM-1) records a sequence of color bitmap images (720×576 pixel—25 fps) on a PC (IEEE-1394 standard). The illuminating system (Shott-Fostec® KL1500 LCD) makes use of an optical fiber ring-light to ensure a uniform illumination on the test surface and it also allows to keep constant both color temperature and light power constant. In order to reduce any undesired reflections, two polarized lens filters are fitted on both ring-light and camcorder lens. TLC are the device used to evaluate the surface temperature and consequently the heat transfer coefficient. For our purpose, we used the SP-40-5 formulation of image therm engineering active from 40 to 45 °C. Crystals are thinned with water and sprayed with an airbrush on the test surface. Afterwards, a water base black paint is sprayed to obtain a black background surface. In steady state tests, the electric heater is glued over the black paint.

2.2. Test section geometry

A test model was appositely designed and built (Giglitto [12]) to simulate typical design conditions for a real cooling channel of gas turbine blade. For tests to be run at low pressure (20–40 kPa), the test section geometry was scaled up by a factor of about 10. The system consists of a smooth PMMA (poly methyl methacrylate) channel, 1500 mm long, with a rectangular passage section, as shown in Fig. 3; its width is fixed to 40 mm, while height can be adjusted between 13.3 and 40 mm, corresponding to aspect ratios from 1 to 3. Wall thickness was chosen so as to allow even very slow transient tests, following design criteria shown by Graham and Rhine in [13]. Two of the four surfaces which generate the section (surfaces 1 and 3) are fully instrumented with temperature and pressure probes, the other two are totally clear and transparent so as to permit the optical access necessary to record TLC images. Ribs are applied on surfaces 2 and 4, while TLC are sprayed only on surface 4 (see Fig. 4).

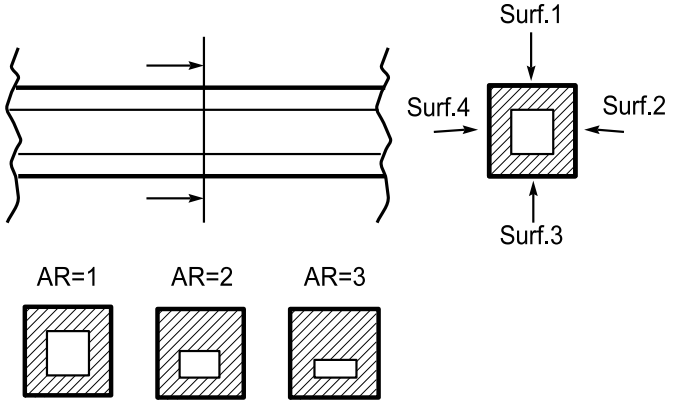

Fig. 3. Test section.

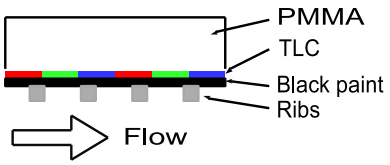

Fig. 4. TLC application.

2.3. Experimental procedures

TLC transient technique has been employed in the present study; only a brief review of the method will be here provided, focusing on those aspects relevant to the performed experiments. Some more detailed descriptions of the technique, which is by now widely well-known and used, can be found in Camci [14] and Ireland et al. [15].

To correctly apply TLC transient technique, the test model must be kept at constant temperature and then quickly exposed to a high temperature flow. Therefore, the air circuit must be previously warmed up. When air temperature reaches about 70–80 °C in the by-pass circuit, the 3-way valve can be switched, so as to allow the air to pass through the test model. Temperature and pressure information are automatically recorded in separate files into the PC, and the camcorder starts recording frames. The test stops when all the liquid crystals reach the blue color. The normal surface temperature response of the PMMA substrate under a step change in fluid temperature is given by the familiar equation:

$$T_w = T_{w0} + (T_a - T_{w0})\left[1 - e^{\frac{h^2 t}{\rho c k}}\operatorname{erfc}\left(\frac{h\sqrt{t}}{\sqrt{\rho c k}}\right)\right] \quad (1)$$

The exact heat transfer coefficient distribution on the test surface can be calculated from Eq. (1), post-processing time–color response over the recorded surface. [16] report five mathematical methods, derived from Eq. (1), to calculate heat transfer coefficient when fluid temperature change is not quick enough. A "Series of Steps" method is used because of its accuracy and small computational time requirements.

2.4. TLC calibration

Color–temperature response of TLC was achieved in a steady state calibration with the successive isotherm method. The calibration setup (see Fig. 5) is made by a

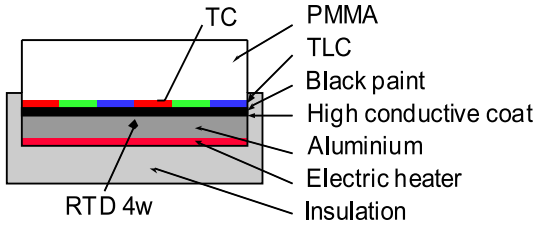

Fig. 5. TLC calibration setup.

70 mm deep PMMA block sprayed with TLC and then with black background paint, as in the experimental setup. Heat is provided by an electric heater glued to an aluminum plate. In order to reduce surface contact resistance, a liquid chrome solution is applied between aluminum plate and black paint. The camcorder and illuminating system too are placed at the same distance and inclination as in the real test. TLC temperature is measured inside the aluminum plate by a four wire RTD and a T-type thermocouple (TC) flush mounted on the PMMA surface before TLC application.

3. Results

At room conditions, TC and RTD measure the same temperature; during the test the RTD always reads 0.2 °C more than TC. This discrepancy is probably due to both a constant heat flux from heater to PMMA and to a small contact resistance between probes and surfaces. Color–temperature response was obtained by using the TC temperature, because of its proximity to TLC layer, but RTD presence was anyway necessary to guarantee TC readings validity. In Fig. 6, hue and red intensity levels vs. temperature are shown, as obtained in several tests. An uncertainty band of 0.1 °C is obtained in hue values, and below 0.1 °C for the red intensity peak. HTC evaluation by means of TLC transient technique needs only one boundary condition. The performed calibration allows to choose any desired hue value between 0.05 and 0.25

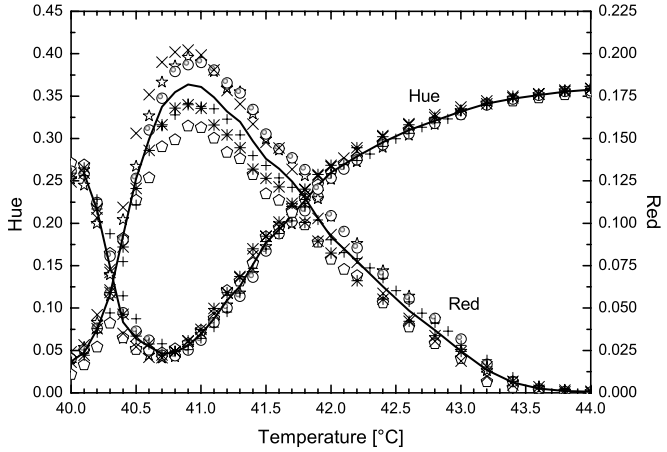

Fig. 6. Hue and red vs. temperature—different performed tests.

Table 1
Ribbed channel test conditions

Aspect ratio	Reynolds	D_h (m)	P/e	e/D_h
1	22,500–59,000	0.04	15.35	0.05
2	24,600–60,500	0.027	15.35	0.075
3	23,500–53,700	0.02	15.35	0.1

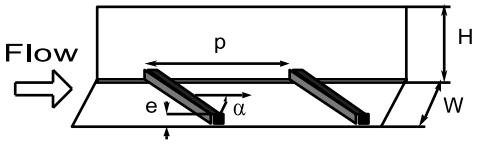

Fig. 7. Geometric parameters.

(40.8–42.0 °C) or the red intensity maximum (40.9 °C) as the required boundary condition.

3.1. Test conditions

First tests were performed without ribs, in a square smooth duct. A very simple geometry was chosen because of the full availability of comparison data concerning both pressure losses and heat transfer coefficients, so as to validate the test apparatus and the data reduction procedure. Then, ribbed channels were investigated at different flow conditions and aspect ratios, as reported in Table 1, following nomenclature defined in Fig. 7. In all performed tests, ribs are square section (2 mm side) prisms, located on two opposite walls and inclined at $\alpha = 60°$. The aspect ratio range was selected as to be representative of real blade internal channels: while the hydraulic diameter was changing, the rib height was kept constant, thus simulations were performed for different e/D_h. Such a choice was retained significant to simulate actual geometries, as in the manufacturing of the rib dimensions in blades are likely to be equal even in different ducts. The scale factor of about 10 would yield to a constant rib height of about 0.2 mm, which is a realistic value.

4. Experimental uncertainty

The uncertainty analysis was performed following the standard ANSI/ASME PTC 19.1 [17] based on the Kline and McClintock method [18]. The individual contributions to the uncertainties of the single parameters for each of the measured physical properties are summarized in Table 2.

5. Experimental results and discussion

To correctly compare experimental results with correlation data of Han in [5] and [3], the following definition of friction factor was adopted:

$$f = \frac{\mathrm{d}p}{\mathrm{d}x}\frac{D_h}{2\rho c^2} = \frac{\Delta p}{\frac{1}{2}\rho c^2 \frac{4L}{D_h}} \tag{2}$$

Table 2
Uncertainty analysis

	Variable	Uncertainty (%)
d	Hole diameter	3.0
$\sqrt{\rho ck}$	PMMA properties	5.0
Δt	Time accuracy	1.1
T	Air temperature	0.5
T_{w0}	Initial temperature	0.2
$\dot{m}$	Mass flow rate	2.0
Δp	Differential pressure	0.2
μ	Air viscosity	1.2
ρ	Air density	0.5
h	Heat transfer coefficient	9.7
Re	Reynolds number	5.5
f	Friction factor	5.4

The main hypothesis, on which friction factor measurement is based, is the absence of heat transfer (which could cause additional total pressure variations): thus, f was determined in cold tests, carried out at ambient temperature, separately from heat transfer tests.

Reynolds number definition was based on the mean mainstream velocity in the duct:

$$Re_{D_h} = \frac{\dot{m} D_h}{S\mu} \tag{3}$$

This Reynolds number was used as a reference in our experimental tests. Similar definition was used to evaluate Nusselt number:

$$Nu_{D_h} = \frac{\bar{h} D_h}{k} \tag{4}$$

where $\bar{h}$ is the heat transfer coefficient mean value measured on the wall surface, and Stanton number

$$St = \frac{\bar{h} S}{\dot{m} c_p} \tag{5}$$

5.1. Smooth channel

Heat transfer coefficient was measured at locations between $x/D_h = 28.5$ and $x/D_h = 30.5$, so as to assume fully developed flow conditions (see Fig. 8). Concerning flow temperature, two micro-thermocouples were located at the two measurement zone ends. Transient TLC method would require the exact knowledge of air temperature in each section, thus it was assumed a linear variation along the duct. Such assumption appears even more acceptable as, due to the adopted flow conditions, air temperature only slightly changes inside measurement section (usually less than 1 °C).

On the other hand, friction factor was evaluated by measuring pressure losses between section at $x/D_h = 12.0$ and $x/D_h = 30.5$. This choice allows to contemporarily consider differential values big enough with respect to instruments accuracy and avoid entrance effects. In all tests flow Mach number was very low (below 0.1), thus compressibility effects on pressure variations are assumed negligible. In a single case, several pressure taps were located between two subsequent ribs, but the periodical pressure variations were extremely small and could be neglected and attributed to the experimental uncertainties.

Let consider now experimental results: in Figs. 9 and 10 Nusselt and friction factor values are plotted against Reynolds number. In both cases, behaviors are coherent with available literature data; Dittus-Boelter correlation with

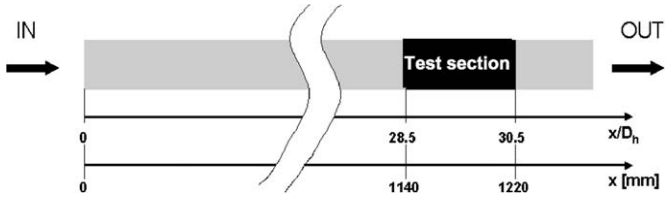

Fig. 8. Smooth channel heat transfer measurement zone.

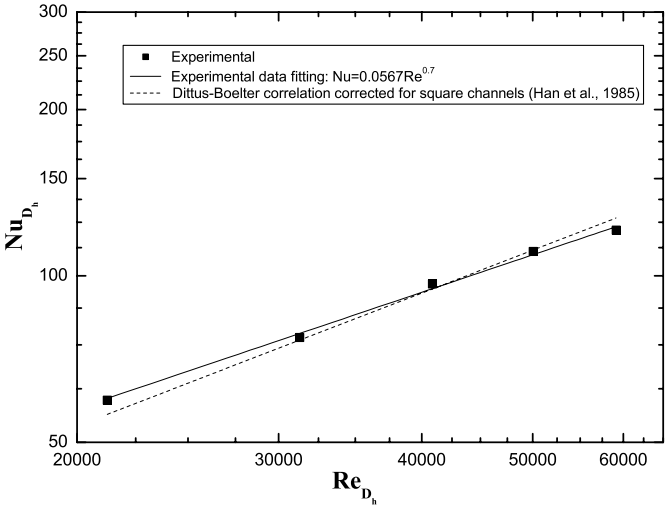

Fig. 9. Nusselt values for smooth channel.

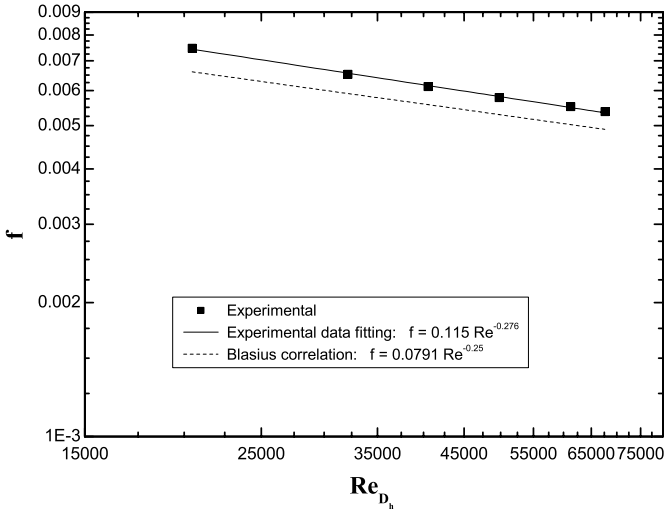

Fig. 10. Friction factor for smooth channel.

the correction for square channel proposed by Han [3] was adopted as a comparison for Nu_{D_h}, while Blasius correlation (as reported in Rohsenow et al. [19]) was used to validate results in terms of friction factor. In the latter, the dependence on Reynolds is very close to the correlation (-0.0276 against -0.0250), while a vertical shift appears, causing a small overestimation. It should be due to the inherent nature of the correlation, which was inferred from tests on circular ducts, which usually show lower pressure losses. In more details, square channels, essentially because of their shape, promote the formation of corner vortices: such secondary flows necessarily determine an increase in the friction factor; probably even the small difference in Reynolds exponent could be attributed to this effect.

To sum up this part, the agreement of results with literature available correlations, commonly employed in turbomachinery design, is retained good in terms of both *Nu* and *f*, thus validating the experimental setup and the data reduction procedure.

5.2. Ribbed channel

Ribbed channel constitutes the main part of the experimental work. One of the goals is to show the aspect ratio influence on heat transfer and pressure losses. With reference to Fig. 11, "B" measurement zone was investigated to study fully developed flow heat transfer performances. Due to the low thermal capacity of PMMA, similarly to the smooth channel, air temperature changes only a little while it passes through the considered length, then allowing to assume a linear variation between the temperature values measured at inlet and outlet.

On the other hand, "A" measurement zone was studied to investigate the variation of heat transfer coefficient due to entrance effects. Such influence should worth an accurate analysis, as cooling geometries commonly feature short ducts, with curves and sharp passage area variations. Even if *Nu* values at the entrance depends strongly on the specific inlet geometry, it is however interesting to expand on the qualitative influence of Reynolds and aspect ratio on heat transfer in such zone. As previously suggested, it is important to understand how much preventive is, for different aspect ratios, to assume fully developed flow for *Nu* estimation during cooling channel design.

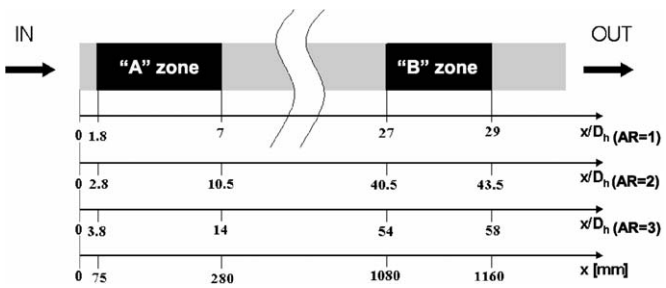

Fig. 11. Ribbed channel heat transfer measurement zone.

Concerning friction factor, it was calculated by measuring the pressure losses between $x = 480$ mm and $x = 1220$ mm, so as to allow the flow to develop and obtain values sufficiently higher than pressure sensors accuracy.

As well known, the heat transfer coefficient on a ribbed surface is strongly influenced by the presence of secondary flows generated by the ribs themselves. Fig. 12, which shows the heat transfer coefficient map over the ribbed wall for the three studied configurations at $Re_{D_h} = 30,000$, highlights that vortices shape and intensity result significantly modified moving from a square to a rectangular section. In particular, while reattachment zone after each rib is clear for AR = 1, it widens up to show an evident deformation for AR = 3. Such behavior could be related to the interference of vortices originating on the two opposite ribbed walls, which is low in the square section and progressively increase as they become closer (Han and Park [5]). As a result, even the heat transfer in the upper area in front of each rib becomes higher, and they look more and more like lighted matches burning in the wind.

A deeper analysis of every single aspect ratio will be now presented, after a due specification: measurements made by Han in [4,5] were obtained locating several thermocouples on the central line of the ribbed wall, then reported data are representative only of such area. TLC technique, being able to provide a very detailed local heat transfer coefficient

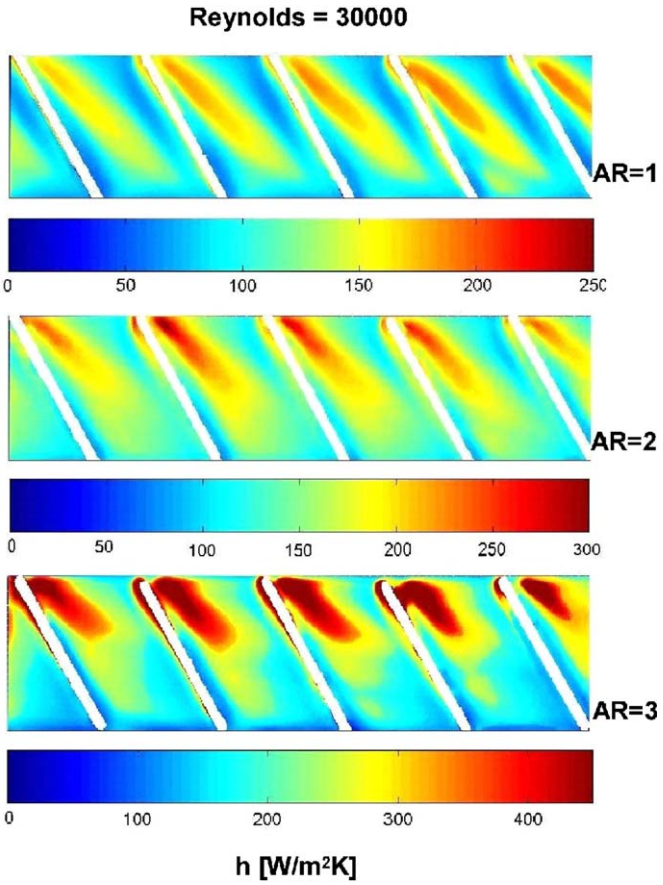

Fig. 12. Aspect ratio effect on heat transfer.

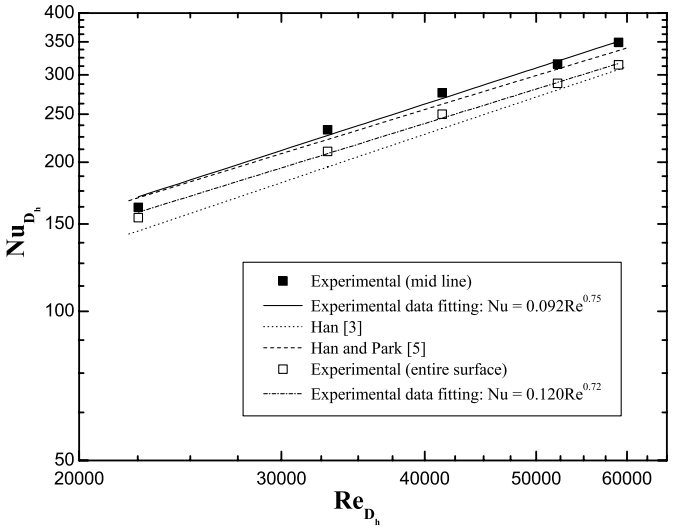

Fig. 13. Calculated Nusselt: comparison with correlations for AR = 1.

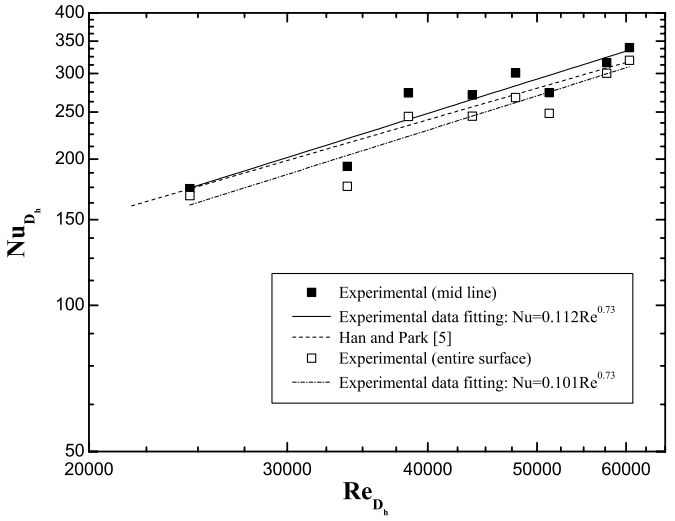

Fig. 14. Calculated Nusselt: comparison with correlation for AR = 2.

distribution over the whole surface, allowed to obtain more accurate measurements. To properly compare calculated data with correlations, Nusselt was evaluated both as an average on the entire area and only on the central zone of the test surface.

Fig. 13 shows the comparison between performed measurements in the square channel (AR = 1) and values proposed by two separate correlations by Han. The accord is not very good with data from [3], developed appositely for square channels, while results looks extremely similar with respect to the second correlations from [5], claimed to be valid for ducts with aspect ratio from 1/4 to 4. It should not surprise that the second one (which itself has a discrepancy with the other for the same AR), later published, appears more accurate; such correlation has been widely used to give correct estimations and compare heat transfer performances of different channels. In addition, it is possible to note the sensible difference between midline and entire area values: for the Reynolds range considered, data relative to central area show everywhere higher Nusselt values. As depicted in Fig. 12, this is due to the presence of ribs generated secondary flows which determines significant differences in heat transfer between various zones: thus considering only the centerline could yield to a global overestimation of heat transfer performances.

Comparison between correlation and experimental results for AR = 2 are reported in Fig. 14; remarks are similar to those previously claimed, again results are very close to performed tests values. Data fitting slope results little different, but this aspect could probably depend on the scattering due to measurement uncertainty. Again, the spatial disuniformity in the heat transfer due to the ribs generated vortices are significant, and values taken from the central line differ from the whole area data.

To end up with heat transfer tests, Fig. 15 is reported. In addition to the considerations already exposed for the other geometries, a new relevant aspect is revealed by these

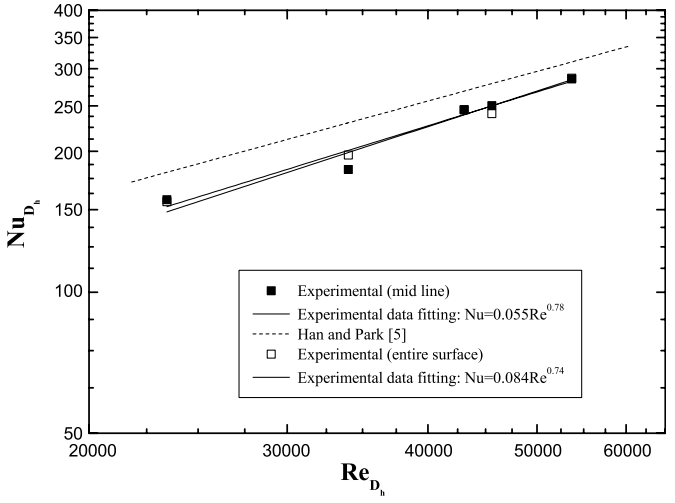

Fig. 15. Calculated Nusselt: comparison with correlation for AR = 3.

results, i.e., no big differences are evidenced varying the investigated area; this because such configuration shows a fairly uniform heat transfer coefficient distribution, thus distinct area averages are very similar. The increased uniformity should be caused by the very stretched passage section which compresses each vortex, flattening and enlarging it, so that its effects are felt on the entire surface between two ribs (see Fig. 16).

Before analyzing the friction factor investigations, one last consideration on heat transfer results can be provided, looking at Fig. 17, where all tests measurements are summarized. It is evident at the first glance that most data collapse in a single exponential dependence on Reynolds, regardless of the different aspect ratios (only for one point the distance from such tendency is above 10%). Apart from confirming the validation of experimental setup and procedure, this could suggests that, though the aspect ratio is doubtless a significant dimensionless quantity when not

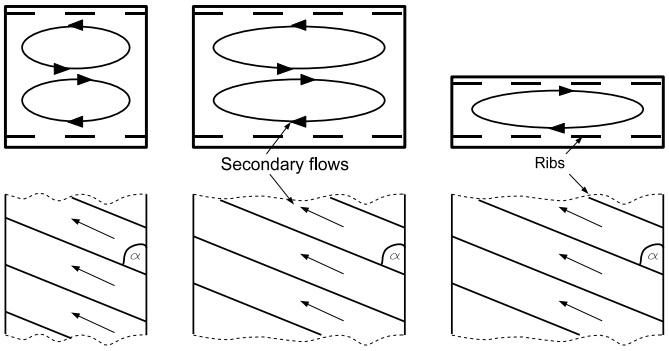

Fig. 16. Secondary flows generated by inclined ribs for different aspect ratios.

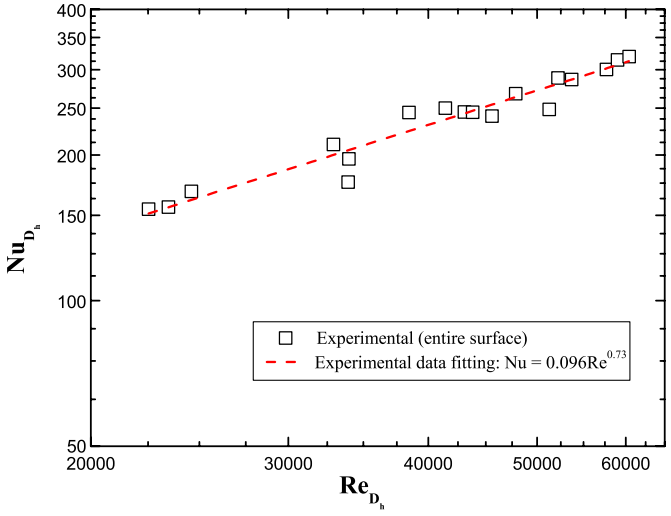

Fig. 17. Nusselt values for all aspect ratios and performed tests.

all walls are rib-roughened, as it determines the fraction of ribbed area, its presence as an active parameter in heat transfer correlations (as in [5]) for such geometry may not be necessary. In more details, tested configurations featured different values for AR but also for e/D_h, with a constant combination of $\frac{e}{D_h}\frac{1}{AR+1}$, thus expressed consideration may not be generalized; however, the constant of e in different aspect ratios, as already reported, could have a practical validity.

Considering pressure losses estimation, Fig. 18 shows results of friction factor measurements, which are compared with the correlation in [5]. As clearly depicted, obtained values for $AR = 1$ and $AR = 2$ result about 10% greater than data from [5] and the agreement is excellent for $AR = 3$, while f keeps almost independent on Reynolds for all geometries.

As expected, the friction factor sensibly increases with the aspect ratio, moving from the square to the rectangular channel. Similarly to what happens with turbulent flows on rough surfaces, when the aspect ratio increases while the rib height is constant, the "roughness" e/D_h and then the friction factor become higher. Even the loss independence on Reynolds is coherent with the turbulent nature of the flow.

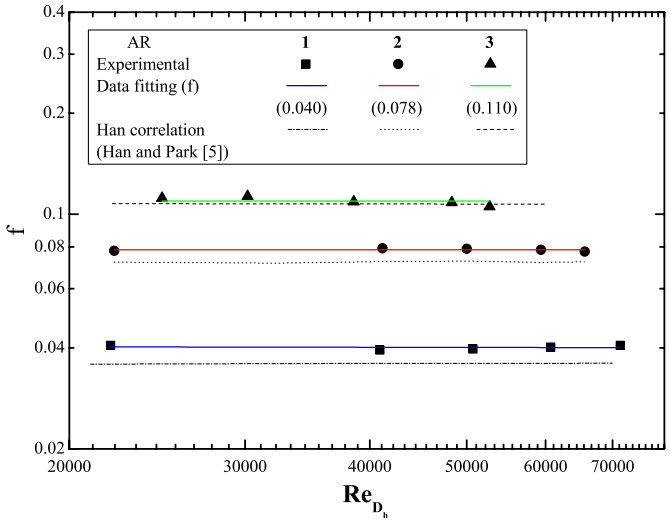

Fig. 18. Friction factor results compared with correlations for all tests.

5.3. Entrance effects

Ribbed channel in turbine blade cooling systems are usually not long enough to reach fully developed flow conditions; moreover, in multi-pass geometries are common curves and setting plates, which further alter coolant flow. Thus, it was chosen to investigate the entrance region for a distance representative of a real cooling duct, so as to evaluate the influence of entrance effects on heat transfer.

In Fig. 19, Nusselt in different locations at the entrance region is reported for the three considered aspect ratio (referred to the fully developed flow Nusselt—taken from previously experimental results). The graphs show that at the very beginning heat transfer is decreased of about 20–25% for all cases; afterwards, the Nusselt starts to increase up to exceed values measured far from the entrance.

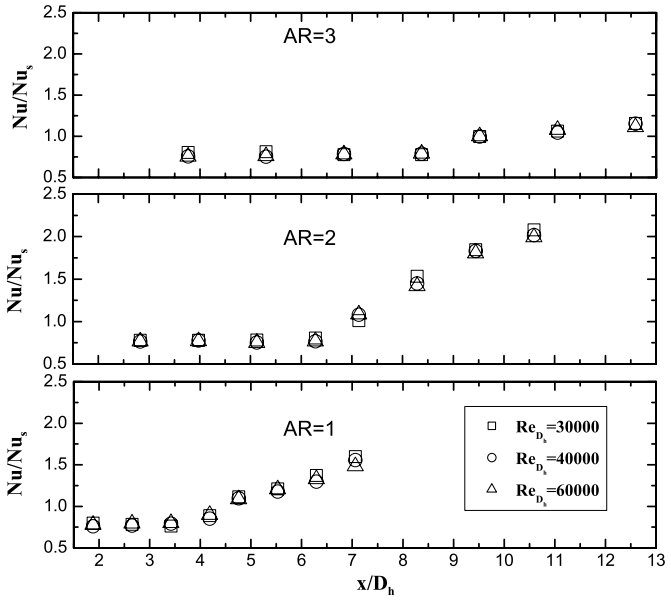

Fig. 19. Nusselt measurements at entrance region.

This would suggest that in an intermediate zone (not investigated) the heat transfer coefficient will have to decrease until to reach the fully developed flow conditions (similar considerations were already reported by the recent numerical works of Jang et al. [20] and Al-Qahtani et al. [21]). In addition, it is necessary to note that for AR = 1 and AR = 2, the average heat transfer in the entrance region results globally higher than in farther zones, respectively, 4–6% and 15–20%. Differently, in the channel with AR = 3 very low values at the beginning are not compensated by the subsequent increase, thus the average is now 5–6% lower. Because of the stretched passage section, swirl effect is predominant with respect of boundary layer separation, thus ribs act more as grooves, inside which the air flows, than as turbulators. It is though necessary to specify again that these aspects are revealed by the particular choice of a constant e, which yields to a blockage of 30% in the case of AR = 3.

To better understand the Nusselt growth at the entrance, it is useful to consider the influence of inclined ribs on the flow. Apart from breaking the boundary layer and distorting streamlines, phenomena which happen also for orthogonally located ribs ($\alpha = 90°$), inclined ribs usually determines two counter-rotating vortices (as in [5] and in Fig. 16). Such secondary flows originate because the fluid closest to the wall, encountering the rib, is deflected towards the smooth wall and causes an opposite flow at the channel center, thus creating the two above mentioned vortical structures. The progressive increase of the heat transfer, registered by Fig. 19, is caused just by the strengthening of secondary flows as flow proceeds inside the channel, up to the attainment of fully developed flow conditions. Moreover, another cause could be the flow contraction in the very first diameters due to the entrance from the upstream plenum; then, it is likely that the first ribs do not interact significantly with the flow. All such effects strongly contribute to reduce the heat transfer enhancement typical of ribs in the investigated region.

From a design point of view, it is fundamental to be aware of the appreciable overestimation of heat transfer performances in short channels (or however for a significant part of realistic internal ducts), whenever entrance effects are neglected.

6. Selection criterion

When a real rib-roughened channel has to be designed, the choice for a particular rib geometry derives from a compromise between two conflicting aspects.

Focusing on heat transfer performances, it would suggest to adopt narrow sections: as evident from the previous results (see in particular Fig. 12), heat transfer coefficient can increases up to 100% from AR = 1 to AR = 3 at the same Reynolds (and then with a lower mass flow rate).

On the other hand, friction factor is minimized in square channels, which can allow to save up to three times the pressure losses predicted in case of AR = 3, which is really a lot. Moreover, a higher coolant pressure would require bleeding it from a forward compressor stage, then at higher temperature, with even worsen heat transfer performances.

These are only some of the aspects which have to be taken into account when the most fitted cooling system has to be designed. To the best of authors' knowledge, selection criterion commonly employed in such cases refers to [11]. The main problem, which arises when using it for turbine blade cooling channels, is the assumption of the same inlet air density and temperature for the smooth and the ribbed channel. In real cooling geometries, such hypothesis is usually not verified, for some of the reason above expressed. Passing from a smooth to a ribbed channel in fact, for a fixed outlet pressure, the increased friction factor requires bleeding air downstream in the compressor, then provided at both higher temperature and density. From these and similar considerations, it was decided to search for a renewed selection criterion, able to satisfy gas turbine cooling systems exigencies.

Generally speaking, coolant will be bled at a pressure ratio:

$$\beta = \frac{p_c}{p_a} \tag{6}$$

corresponding to a coolant temperature:

$$T_c = T_a + \frac{T_a}{\eta_c}\left(\beta_c^{\frac{\gamma-1}{\gamma}} - 1\right) \tag{7}$$

Surface stresses can be calculated as:

$$\tau_w = \frac{D_h}{4}\frac{dp}{dx} = \frac{fM^2}{2\rho} \tag{8}$$

where M refers to the mass velocity. Considering one smooth and one ribbed configuration, their pumping power ratio is then expressed as:

$$\frac{W}{W_{sm}} = \frac{\tau_w Ac}{(\tau_w Ac)_{sm}} = \frac{fAM^3}{\rho^2}\frac{\rho_{sm}^2}{f_{sm}A_{sm}M_{sm}^3} \tag{9}$$

which, considering the perfect gas relation to eliminate density, becomes:

$$\frac{W}{W_{sm}} = \frac{f}{f_{sm}}\frac{A}{A_{sm}}\left(\frac{M}{M_{sm}}\right)^3\left(\frac{\beta_{csm}}{\beta_c}\right)^2\left(\frac{T_c}{T_{csm}}\right)^2 \tag{10}$$

Similarly, the heat transfer ratio can be expressed introducing Stanton number as:

$$\frac{Q}{Q_{sm}} = \frac{h}{h_{sm}}\frac{A}{A_{sm}}\frac{\left(T_w - \frac{1}{2}(T_c + T_{co})\right)}{\left(T_{wsm} - \frac{1}{2}(T_{csm} + T_{cosm})\right)} = \frac{St}{St_{sm}}\frac{M}{M_{sm}}\frac{A}{A_{sm}}\frac{\left(T_w - \frac{1}{2}(T_c + T_{co})\right)}{\left(T_{wsm} - \frac{1}{2}(T_{csm} + T_{cosm})\right)} \tag{11}$$

Suppressing M/M_{sm} between Eqs. (10) and (11), an expression which compare two configurations is obtained, like the one in [11], but taking into account coolant different pressure and temperature in the two cases:

$$\frac{W}{W_{sm}} = \frac{f}{f_{sm}}\left(\frac{A_{sm}}{A}\right)^2\left(\frac{\beta_{csm}}{\beta_c}\right)^2\left(\frac{T_c}{T_{csm}}\right)^2\left(\frac{St_{sm}}{St}\right)^3 \cdot \left[\frac{Q}{\left(T_w - \frac{1}{2}(T_c + T_{co})\right)}\right]^3\left[\frac{\left(T_{wsm} - \frac{1}{2}(T_{csm} + T_{cosm})\right)}{Q_{sm}}\right]^3 \tag{12}$$

Such formulation, even if itself complete, could be much more interesting if expressed including turbomachinery cooling typical quantities for performances evaluation, like efficiency and effectiveness, respectively, defined as:

$$\epsilon = \frac{T_{co} - T_c}{T_w - T_c}, \quad \phi = \frac{T_g - T_w}{T_g - T_c} \tag{13}$$

A good cooling system should be designed so as to exploit at most the coolant temperature (thus reducing the mass flow rate), and then very efficient, while keeping the blade as cold as possible, i.e., with a high effectiveness.

Using the efficiency definition, the heat transfer Q of Eq. (11) can be written in another form:

$$Q = \dot{m}_c c_{pc} \epsilon (T_w - T_c) \tag{14}$$

which substituted in Eq. (12) yields to:

$$\frac{W}{W_{sm}} = \frac{f}{f_{sm}}\left(\frac{A_{sm}}{A}\right)^2\left(\frac{\beta_{csm}}{\beta_c}\right)^2\left(\frac{T_c}{T_{csm}}\right)^2 \cdot \left(\frac{St_{sm}}{St}\right)^3\left(\frac{\dot{m}_c \epsilon (2 - \epsilon_{sm})}{\dot{m}_{csm}\epsilon_{sm}(2 - \epsilon)}\right)^3 \tag{15}$$

On the hot side of the cooling duct, the heat transfer can be calculated as:

$$Q_g = \dot{m}_g c_{pg} St_g \frac{A_b}{S_g}(T_g - T_w) \tag{16}$$

From the thermal balance on the wall, Q and Q_g have to be equal:

$$\dot{m}_c \epsilon = \dot{m}_g \frac{c_{pg}}{c_{pc}}\frac{A_b}{S_g} St_g \frac{T_g - T_w}{T_w - \frac{1}{2}(T_c + T_{co})} = \dot{m}_g \frac{c_{pg}}{c_{pc}}\frac{A_b}{S_g} St_g \frac{\phi}{1 - \phi - \frac{\epsilon}{2}} \tag{17}$$

Combining Eqs. (15) and (17), eventually the final version of the comparison expression is attained:

$$\frac{W}{W_{sm}} = \frac{f}{f_{sm}}\left(\frac{A_{sm}}{A}\right)^2\left(\frac{\beta_{csm} T_c}{\beta_c T_{csm}}\right)^2\left(\frac{St_{sm}}{St}\right)^3 \cdot \left(\frac{\phi(2 - \epsilon_{sm})}{\left(1 - \phi - \frac{\epsilon}{2}\right)}\frac{\left(1 - \phi_{sm} - \frac{\epsilon_{sm}}{2}\right)}{\phi_{sm}(2 - \epsilon)}\right)^3 \tag{18}$$

To correctly utilize the previous equations, the relation between β_c and f need to be clearly quantified. Setting the discharge pressure p_d and putting together Eqs. (2) and (6), such dependence can be written as

$$f = \frac{(\beta_c p_a - p_d)\rho_c D_h}{2M^2 L} \tag{19}$$

and introducing Eq. (3) and perfect gas relation, it becomes

$$f = \frac{\beta_c p_a (\beta_c p_a - p_d) D_h^3}{2RL\mu^2 Re^2 T_c} \tag{20}$$

As f can be easily evaluated by means of correlations, it is now possible to correctly compare two systems: once Reynolds is set, and then β_c and T_c are calculated, performances can be estimated for the possible configurations so as to choose the best one.

6.1. Criterion application

On the basis of performed experiments, the three investigated geometries will be now compared by means of Eq. (18). Heat transfer coefficients and friction factors were calculated with the correlations for ribbed channels inferred by presented tests, while smooth channel data were acquired by available literature. Before reporting the application, it is necessary start reminding that experimental tests were performed at constant e, thus relevant considerations are always referred to this condition.

To carry out the comparison, apart from setting the same pumping power and heat transfer area, the following quantities were fixed: ambient conditions, compressor efficiency and discharge pressure. Several different results could be presented; it was chosen to plot the dependence of mass flow rate on efficiency for all tests and on effectiveness for a given value of Reynolds in all geometries.

Fig. 20 reports, for each tested aspect ratio, efficiency of each configuration as a function of coolant mass flow rate, both referred to the correspondent smooth channel values, always for the same pumping power. As expected, efficiency decreases as flow increases, as a higher $\dot{m}$ generally implies a lower outlet temperature. It appears that square ribbed channels are often more efficient than smooth ones: they would allow to increase coolant flow up to 10–15%, thus effectiveness, and then maximum cycle temperature

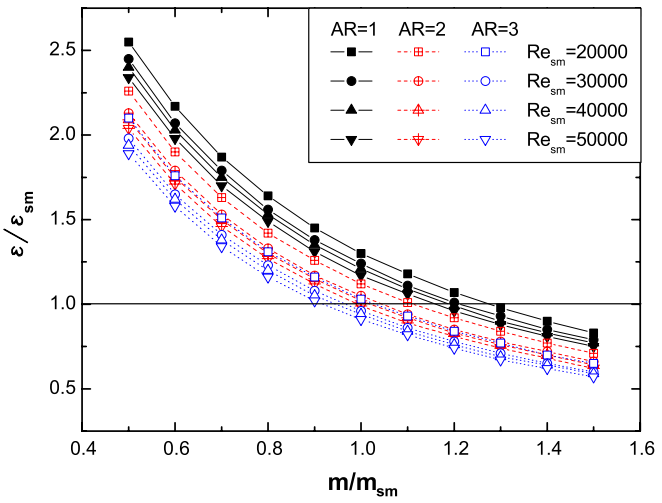

Fig. 20. Efficiency ratio as a function of mass flow rate for different aspect ratios and Reynolds, calculated @ $\epsilon_{sm} = 0.25$.

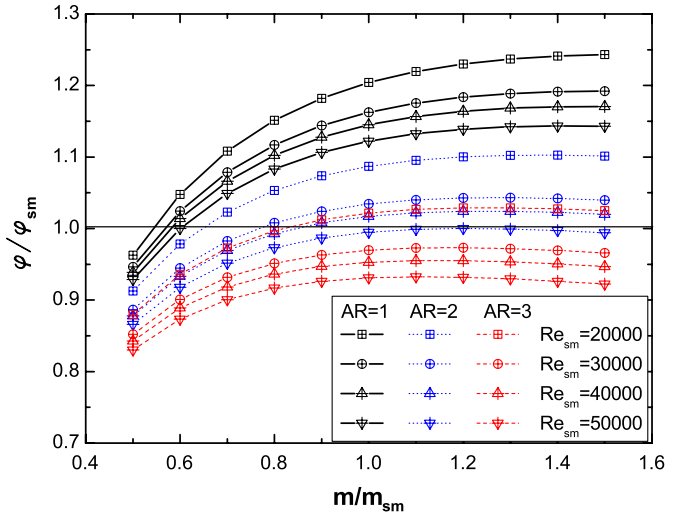

Fig. 21. Effectiveness ratio as a function of mass flow rate for different aspect ratios and Reynolds, calculated @ $\epsilon_{sm} = 0.25$ and $\phi_{sm} = 0.1$.

with the same wall temperature and pumping power (from Eq. (18)). From the same graph, we could infer that, in terms of efficiency, AR = 2 is convenient only for $\dot{m}/\dot{m}_{sm} \leqslant 1$, while AR = 3 appears less efficient already at $\dot{m}/\dot{m}_{sm} \approx 0.9$.

Let now consider Fig. 21, where cooling effectiveness ratio is represented for the various aspect ratios as a function of mass flow rate ratio (always with the same pumping power, from Eq. (18)). Square ribbed channel behaves again better than each other in the plotted range and, what is more, better than the smooth channel for $\dot{m}/\dot{m}_{sm} \geqslant 0.6$. It is then possible with it to maintain the same blade temperature with hotter gases. Other aspect ratios appear slightly better (AR = 2) or significantly worse (AR = 3).

Reported results reveal just some of the opportunities provided by the utilization of the presented selection criterion. Different comparisons could be drawn by setting different boundary conditions, e.g., changing heat transfer area ratio or pumping power ratio, or focusing on other design aspects.

7. Conclusions

The paper presents the results of an experimental study concerning performances at various aspect ratios of rib-roughened channels (ribs inclined at $\alpha = 60°$), commonly employed in turbine blade cooling systems. Experimental tests were performed with transient TLC technique on a PMMA model, properly designed to reproduce large-scale cooling ducts with different aspect ratios (AR = 1, 2, 3). To validate the test model and the data acquisition and reduction procedure, a smooth channel was initially studied and relative results were found in good agreement with common correlations for heat transfer and pressure losses. A novel aspect of this study is represented by the investigation of the initial region, so as to evaluate the entrance effect influence on heat transfer coefficient of such area. Performed tests showed that, for all geometries, there is a first part (2–3 hydraulic diameters) where Nusselt is 20–25% below the value reached for fully developed flow conditions. Then it increases and exceeds such value up to 100% in the AR = 2 channel, even if globally the entrance region shows a moderate raise (maximum 20% for AR = 2). Such behavior significantly differs from the smooth channel case, where there is a monotonous decrease of heat transfer up to the developed conditions. This should warn cooling system designer from the choice of always considering fully developed conditions as a conservative assumption.

Finally, a long dissertation is dedicated to attain a selection criterion for cooling channels, suited for gas turbine systems. Its application yielded to compare global behavior of investigated geometries and to claim that while square ribbed channels always allow to improve cooling system global performances, stretched passage sections can be retained as usually worse (as far as the presented criterion is concerned), as the increase in heat transfer is overcome by the corresponding rise of pressure losses.

Acknowledgement

The authors wish to thank Dr. F. Giglitto for his fundamental support to perform the work.

References

[1] J.C. Han, L.R. Glicksman, W.M. Rohsenow, An investigation of heat transfer and friction for rib-roughened surfaces, Int. J. Heat Mass Transfer 21 (1978) 1143–1156.
[2] R.L. Webb, E.R.G. Eckert, R.J. Goldstein, Heat transfer and friction in tubes with repeated-rib roughness, Int. J. Heat Mass Transfer 14 (1971) 601–617.
[3] J.C. Han, J.S. Park, C.K. Lei, Heat transfer enhancement in channels with turbulence promoters, ASME J. Eng. Gas Turbines Power 107 (1985) 628–635.
[4] J.C. Han, Heat transfer and friction characteristics in rectangular channels with rib turbulators, ASME J. Heat Transfer 110 (1988) 321–328.
[5] J.C. Han, J.S. Park, Developing heat transfer in rectangular channels with rib turbulators, Int. J. Heat Mass Transfer 31 (1988) 183–195.
[6] M.E. Taslim, Convective cooling in non-rotating and rotating channels: experimental aspectsLecture Series 2000-03, von Karman Institute for Fluid Dynamics, 2000.
[7] S.W. Chang, W.D. Morris, Heat transfer in a radially rotating square duct fitted with in-line transverse ribs, Int. J. Thermal Sci. 42 (2003) 267–282.
[8] G. Su, S. Teng, H.C. Chen, J.C. Han, Flow and heat transfer computations in rotating rectangular channels with v-shaped ribs, AIAA J. Thermophys. Heat Transfer (2004) 534–547.
[9] M.E. Taslim, Lengkong A, 45° round-corner rib heat transfer coefficient measurements in a square channel, ASME paper (98-GT-176), 1998.
[10] J.J. Hwang, Measurements of heat transfer and pressure drop in a rectangular channel with repeated perforated ribs of various widths, ASME paper (97-GT-476), 1997.
[11] R. Webb, E. Eckert, R. Goldstein, Generalized heat transfer and friction correlations for tubes with repeated-rib roughness, Int. J. Heat Mass Transfer 15 (1972) 180–184.

[12] F. Giglitto, The use of turbulence promoters in gas turbine cooling systems (in italian). Master thesis. University of Florence, 2003.
[13] D. Graham, J. Rhine, The design of transient wall heating experiments for the determination of convective heat transfer using liquid crystal thermography, ASME Paper (2000-GT-658), 2000.
[14] C. Camci, Liquid crystal thermography, in: Temperature Measurements, Lecture Series 1996-07, von Karman Institute for Fluid Dynamics, 1995.
[15] P.T. Ireland, Z. Wang, T.V. Jones, Liquid crystal heat transfer measurements, in: Measurements Techniques, Lecture Series 1993-05, von Karman Institute for Fluid Dynamics, 1993.
[16] P.T. Ireland, T.V. Jones, Liquid crystal measurements of heat transfer and surface shear stress, Meas. Sci. Technol. 11 (2000) 969–986.
[17] ASME, Measurement uncertainty, In Instrument and Apparatus, vol. ANSI/ASME PTC 19.1-1985 of Performance Test Code. ASME, 1985.
[18] S.J. Kline, F.A. McClintock, Describing uncertainties in single sample experiments, Mech. Eng. 75 (1953) 3–8.
[19] W.M. Rohsenow, J.P. Hartnett, Y.I. Cho, Handbook of Heat Transfer, third ed., McGraw-Hill, 1998.
[20] Y.J. Jang, H.C. Chen, J.C. Han, Flow and heat transfer in a rotating square channel with 45° angled ribs by reynolds stress turbulence model, ASME Paper (2000-GT-0229), 2000.
[21] M. Al-Qahtani, H.C. Chen, J.C. Han, A numerical study of flow and heat transfer in rotating rectangular channels (AR = 4) with 45° rib turbulators by Reynolds stress turbulence model, ASME paper (GT-2002-30216), 2002.